Nonlinear Dyn (2012) 67:1779–1790
DOI 10.1007/s11071-011-0105-4

ORIGINAL PAPER

The bifurcation analysis on the circular functionally graded plate with combination resonances

Yuda Hu · Zhiqiang Zhang

Received: 10 August 2010 / Accepted: 24 May 2011 / Published online: 16 June 2011

Abstract The bifurcation and chaos of a clamped circular functionally graded plate is investigated. Considered the geometrically nonlinear relations and the temperature-dependent properties of the materials, the nonlinear partial differential equations of FGM plate subjected to transverse harmonic excitation and thermal load are derived. The Duffing nonlinear forced vibration equation is deduced by using Galerkin method and a multiscale method is used to obtain the bifurcation equation. According to singularity theory, the universal unfolding problem of the bifurcation equation is studied and the bifurcation diagrams are plotted under some conditions for unfolding parameters. Numerical simulation of the dynamic bifurcations of the FGM plate is carried out. The influence of the period doubling bifurcation and chaotic motion with the change of an external excitation are discussed.

Keywords Functionally graded plate · Combination resonance · Multi-scale method · Universal unfolding · Bifurcation

1 Introduction

Functionally graded material (FGM) is a new type of inhomogeneous composite materials, which are usually made from mixture of metals and ceramics. It is known that ceramics are excellent in heat-resistance and metal has good characteristics in strength and toughness. FGMs were initially designed as thermal barrier materials for aerospace structures. Nowadays, FGMs are being developed for structural components including beams, plates, and shells to satisfy extremely high-temperature conditions.

Since the concept of FGMs [1] was firstly proposed, FGMs, especially their thermo-elastic behavior or buckling behavior have been extensively studied by researchers. Noda [2] provided a comprehensive discussion of thermal stress of FGMs under a steady-temperature field or thermal shock. Praveen and Reddy [3] investigated the static and dynamic thermo-elastic response of functionally graded plates using the finite methods. Liew et al. [4, 5] studied the thermal post-buckling of FGPs with temperature-dependent properties and the post-buckling of piezoelectric FGM plates subjected to thermo-electro-mechanical loading. There are some other works on FGMs research, such as, a theoretical formulation and finite element models for FGPs [6], the feedback control of FGM shells [7], the finite element formulation for a geometrically non-linear thermo-elastic FGM [8], the mechanical and thermal buckling analysis of functionally graded plates [9], etc.

With the increased use of FGM components in engineering, several researchers have focused their attention on investigating the dynamics of FGM components under mechanical load and thermal load. Based

Y. Hu (✉) · Z. Zhang
School of Civil Engineering and Mechanics, Yanshan University, Qinhuangdao 066004, P.R. China
e-mail: huyuda03@163.com

on the first-order shear deformation theory, Praveen and Reddy [10] provided the nonlinear transient thermoelastic analysis of functionally graded ceramic-metal plates subjected to pressure load and thickness varying temperature fields. Ng et al. [11] analyzed the parametric resonance of functionally graded rectangular plates under harmonic in-plane loading. Yang and Shen [12] studied the dynamic responses of initially stressed FGM rectangular thin plates subjected to partially distributed impulsive lateral loads. They considered the influence of an elastic foundation. Also, they [13] analyzed the free vibration parametric resonance of shear deformable functionally graded cylindrical panels subjected to combined static and periodic axial forces in the thermal environment. A three-dimensional solution for the free and forced vibration of simply supported FGPs was provided by Vel and Batra [14] using different plate theories, and Liew et al. [15] carried out the finite element piezothermoelasticity analysis and the active control of FGM plates with integrated piezoelectric sensors and actuators. Allahverdizadeh [16] studied the nonlinear free and forced axisymmetric vibration of a thin circular functionally graded plate and gave the relationship between the free vibration frequencies and vibration amplitudes. Zhao and Liew [17] investigated the nonlinear response of functionally graded ceramic-metal plates under mechanical and thermal loads using the mesh-free kp-Ritz method. He et al. [18] presented the static response and free vibration of metal and ceramic functionally graded shells subjected to mechanical or thermomechanical loading. Hao and Zhang [19] analyzed the nonlinear dynamics of a simply supported functionally graded materials rectangular plate subjected to the transversal and in-plane excitations in a thermal environment. Here, they considered the resonant case is 1:1 internal resonance and principal parametric resonance. Recently, Yang et al. [20] carried out an analysis of the nonlinear vibration of a simply supported functionally graded rectangular plate with a through-width surface crack.

Studies of the nonlinear vibrations and chaos of the plate have been extensively conducted in the past decades. In [21], Sridhar et al. studied the axisymmetric response of a circular plate to a harmonic excitation. The method of multiple scales was employed and internal resonances were found. Hadian and Nayfeh [22] used the method of multiple scales to investigate the axisymmetric response of circular plates in the case of internal resonance. A reduced model based on specifically chosen mode shapes was employed. Feng and Sethna [23] made use of a global perturbation method to study the global bifurcations and chaotic dynamics of thin plate under parametric excitation and obtained the conditions in which Shilnikov type homoclinic orbits and chaos can occur. Chang et al. [24] investigated the bifurcations and chaos of a rectangular thin plate with 1:1 internal resonance. Liu and Chen [25] analyzed the geometrically nonlinear free vibrations of polar orthotropic circular plates using an axisymmetric finite element method. Global bifurcations and chaotic dynamics were investigated by Zhang et al. [26] for a parametrically and externally excited simply supported thin plate. Haterbouch and Benamar [27–29] studied rather complete investigations on the harmonic and axisymmetric nonlinear vibrations of circular plates; the equations of motion were derived from the kinetic and potential energies and the harmonic balance method was employed with one harmonic. Akour and Nayfeh [30] investigated the nonlinear dynamics and bifurcation of orthotropic circular plates with simply supported boundary condition. Zhang et al. [31] carried out an analysis of the multi-pulse Shilnikov type chaotic dynamics of a parametrically and externally excited, simply supported rectangular thin plate using a extended Melinkov method. Recently, the transition from periodic to chaotic vibrations in free-edge, perfect, and imperfect circular plates were analyzed by Touzé et al. [32].

Since the combination resonance of a clamped circular functionally graded plate in the thermal environment has not been studied, in this paper, we investigate the local bifurcation, dynamic bifurcation and chaos of the clamped circular functionally graded plate with combination resonance for two-term harmonic excitations. Material properties of the constituents are graded in the thickness direction according to a power-law distribution. In the framework of classical plate theory, the governing equations of the FGM circular plate are derived via the principle of virtual work. Using Galerkin's procedure, the governing equations can be reduced to a Duffing system. The method of multiple scales is used to obtain a bifurcation equation, and then the fourth-order Runge–Kutta algorithm [33] is utilized to numerically analyze the dynamic bifurcations and chaotic motions of the FGM circular plate subjected to thermal and mechanical loads for the combination resonance.

2 FGM material properties

Consider a thin circular FGM plate subjected to axisymmetric transverse loads under cylindrical coordinates r, θ and z, as shown in Fig. 1. Its initial configuration is undeformed. The plate edge is clamped and immovable in the r direction. The disk has uniform thickness h and is bounded by $z = \pm h/2$ and $r = R$. The plate is excited in a manner which will produce large vibration amplitude. The displacement at any point can be expressed by the radial displacement u and the transverse displacement.

Usually, most of the FGMs are employed in a high-temperature environment and many of the constituent materials may possess temperature-dependent properties. It is assumed that the plate is made from a mixture of ceramics and metals. The bottom surface of the plate is ceramic-rich, whereas the top surface is metal-rich. The materials properties P, such as the Young's modulus E or the coefficient of thermal expansion α, can be expressed as

$$P = P_c V_c + P_m V_m \tag{1}$$

P can also be expressed by a function of temperature [34]

$$P = P_0\left(P_{-1}T^{-1} + 1 + P_1 T + P_2 T^2 + P_3 T^3\right) \tag{2}$$

where P_c and P_m denote the temperature-dependent properties of the ceramics and metals, respectively. P_0, P_{-1}, P_2, and P_3 are the coefficients of temperature T and are unique to the constituent materials.

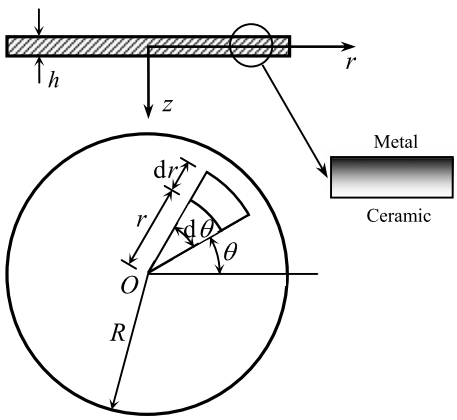

Fig. 1 The model of an FGM circular plate and the coordinate system

V_c and V_m are the ceramics and metal volume fractions and satisfy the following relations:

$$V_c + V_m = 1, \qquad V_c = \left(\frac{2z+h}{2h}\right)^n \tag{3}$$

where n is volume fraction index.

It is assumed that the effective Young's modulus E and thermal expansion coefficient α are temperature-dependent, whereas the mass density ρ, Poisson ratio μ and thermal conductivity κ are independent to the temperature. From (1)–(3), one has

$$E(z,T) = \left(E_c(T) - E_m(T)\right)\left(\frac{2z+h}{2h}\right)^n + E_m(T) \tag{4a}$$

$$\alpha(z,T) = \left(\alpha_c(T) - \alpha_m(T)\right)\left(\frac{2z+h}{2h}\right)^n + \alpha_m(T) \tag{4b}$$

$$\mu(z) = (\mu_c - \mu_m)\left(\frac{2z+h}{2h}\right)^n + \mu_m \tag{4c}$$

$$\rho(z) = (\rho_c - \rho_m)\left(\frac{2z+h}{2h}\right)^n + \rho_m \tag{4d}$$

$$\kappa(z) = (\kappa_c - \kappa_m)\left(\frac{2z+h}{2h}\right)^n + \kappa_m \tag{4e}$$

We assume that the temperature variation occurs in the thickness direction only and one dimensional temperature field is constant in the $r\theta$ plane of the plate. In such a case, the temperature distribution along the thickness can be obtained by solving a steady-state heat transfer equation

$$-\frac{\mathrm{d}}{\mathrm{d}z}\left[\kappa(z)\frac{\mathrm{d}T}{\mathrm{d}z}\right] = 0 \tag{5}$$

The boundary conditions are $T = \Delta T_c$ at $(z = h/2)$ and $T = \Delta T_m$ at $(z = -h/2)$. The solution of this equation can be expressed as polynomial series [35].

3 Equations of motion

Assuming the Poisson ratio μ as a constant and taking into account the thermal effects, the stress strain relationship is as follows:

$$\sigma_r = \frac{E(z)}{1-\mu}\left[\frac{1}{1+\mu}(\varepsilon_r + \mu\varepsilon_\theta) - \alpha(z)\Delta T(z)\right] \tag{6a}$$

$$\sigma_\theta = \frac{E(z)}{1-\mu}\left[\frac{1}{1+\mu}(\varepsilon_\theta + \mu\varepsilon_r) - \alpha(z)\Delta T(z)\right] \quad (6b)$$

Based on the classical Kirchhoff plate theory, the nonlinear strain-displacement relations are

$$\begin{Bmatrix}\varepsilon_r \\ \varepsilon_\theta\end{Bmatrix} = \begin{Bmatrix}\varepsilon_r^0 \\ \varepsilon_\theta^0\end{Bmatrix} + z\begin{Bmatrix}\varepsilon_r^1 \\ \varepsilon_\theta^1\end{Bmatrix} \quad (7)$$

where

$$\begin{Bmatrix}\varepsilon_r^0 \\ \varepsilon_\theta^0\end{Bmatrix} = \begin{Bmatrix}\frac{\partial u_0}{\partial r} + \frac{1}{2}(\frac{\partial w_0}{\partial r})^2 \\ \frac{u_0}{r}\end{Bmatrix}$$

denotes the strain of the middle surface,

$$\begin{Bmatrix}\varepsilon_r^1 \\ \varepsilon_\theta^1\end{Bmatrix} = \begin{Bmatrix}\frac{\partial^2 w_0}{\partial r^2} \\ \frac{1}{r}\frac{\partial w_0}{\partial r}\end{Bmatrix}$$

denotes the curvature of the middle surface and the change of the twist. u_0 and w_0 are the displacements of the middle surface.

The circular functionally graded plate is acted by transverse harmonic load and thermal load. Introducing stress function $\psi(r,t)$ and combining (4), (5), (6), and (7), the nonlinear governing equations of motion for the FGM plate are derived by using the principle of virtual work

$$\frac{\partial^2\psi}{\partial r^2} + \frac{1}{r}\frac{\partial\psi}{\partial r} - \frac{\psi}{r^2} = -\frac{B_1 h}{2r}\left(\frac{\partial w_0}{\partial r}\right)^2 \quad (8)$$

$$\begin{aligned}&\left(\frac{h^3 B_2^2}{B_1(1-\mu^2)} - \frac{h^3 B_4}{1-\mu^2}\right)(\nabla^4 w_0) + \frac{1}{r}\frac{\partial}{\partial r}\left(\psi\frac{\partial w_0}{\partial r}\right)\\ &\quad + \frac{hB_2}{B_1(1-\mu^2)}\left[r\frac{\partial^4\psi}{\partial r^4} + (5-\mu)\frac{\partial^3\psi}{\partial r^3}\right.\\ &\quad \left. + \frac{3-2\mu}{r}\frac{\partial^2\psi}{\partial r^2} + \frac{\mu}{r^2}\left(\frac{\partial\psi}{\partial r} - \frac{\psi}{r}\right)\right]\\ &\quad + \frac{h^2 B_2}{1-\mu^2}\left[\frac{\partial w_0}{\partial r}\frac{\partial^3 w_0}{\partial r^3} + \frac{(2-\mu)}{r}\frac{\partial w_0}{\partial r}\frac{\partial^2 w_0}{\partial r^2}\right.\\ &\quad \left. + \left(\frac{\partial^2 w_0}{\partial r^2}\right)^2\right] + P_z\\ &= I_0\frac{\partial^2 w_0}{\partial t^2} + \delta\frac{\partial w_0}{\partial t}\end{aligned} \quad (9)$$

$$u_0 = \frac{r}{B_1 h}\frac{\partial\psi}{\partial r} - \frac{\mu}{B_1 h}\psi + \frac{B_2 h}{B_1}\frac{\partial w_0}{\partial r} + \frac{rB_3}{B_1} \quad (10)$$

where P_z is the transverse excitation, δ is the damping coefficient, t is time variation, $I_0 = \int_{-h/2}^{h/2}\rho(z)\,\mathrm{d}z$ is the area mass density. B_i $(i = 1\text{–}4)$ are constants which depend on the thermal properties and the volume fraction index:

$$B_1 = \int_{-h/2}^{h/2}\frac{E(z)}{h}\,\mathrm{d}z$$

$$B_2 = \int_{-h/2}^{h/2}\frac{E(z)}{h^2}z\,\mathrm{d}z$$

$$B_3 = \int_{-h/2}^{h/2}\frac{E(z)\alpha(z)\Delta T(z)}{h}\,\mathrm{d}z$$

$$B_4 = \int_{-h/2}^{h/2}\frac{E(z)}{h^3}z^2\,\mathrm{d}z$$

4 Local bifurcation

The plate edge is clamped and immovable in r direction. The boundary conditions can be expressed: at $r = 0, u_0 = \frac{\partial w_0}{\partial r} = 0$; at $r = R, u_0 = w_0 = \frac{\partial w_0}{\partial r} = 0$. The transversal excitations acted on the FGM plate are represented by $q_1(r)\cos\omega_1 t$ and $q_2(r)\cos\omega_2 t$. Here, ω_1 and ω_2 are the frequencies of the transversal excitations. Thus, we write w_0 as follows:

$$w_0 = f(t)\left[1 - 2\left(\frac{r}{R}\right)^2 + \left(\frac{r}{R}\right)^4\right] \quad (11)$$

where $f(t)$ is the amplitude of the first mode.

Substituting (11) into (8)–(10) and introducing small parameter ε, the Duffing dimensionless equation of transverse motion of the FGM plate is

$$\ddot{g} + g = -\varepsilon\tilde{\eta}_1\dot{g} - \varepsilon\tilde{\eta}_2 g^3 + \eta_3(q_1\cos\Omega_1\tau + q_2\cos\Omega_2\tau) \quad (12)$$

where $g(\tau) = f/h$ is the dimensionless amplitude, $\tau = \omega_0 t$ is the dimensionless time variation. The coefficients are

$$\tilde{\eta}_1 = \frac{\eta_1}{\varepsilon}, \qquad \tilde{\eta}_2 = \frac{\eta_2}{\varepsilon}$$

$$\omega_0^2 = \frac{320}{3I_0R^4}\left[\frac{h^3 B_4}{1-\mu^2} - \frac{h^3 B_3}{B_1(1-\mu^2)}\right] + \frac{20B_3 h}{3R^2}$$

$$\eta_1 = \frac{\delta}{I_0\omega_0}, \qquad \eta_2 = \frac{h^3 B_1}{I_0 R^4\omega_0^2}\left[\frac{(50-30\mu)}{9(1-\mu)} - \frac{40}{21}\right]$$

$$\eta_3 = \frac{5q_1}{3I_0 h\omega_0^2}, \qquad \eta_3 = \frac{5q_2}{3I_0 h\omega_0^2}$$

$\Omega_1 = \frac{\omega_1}{\omega_0}$, and $\Omega_2 = \frac{\omega_2}{\omega_0}$ denote the dimensionless excitation frequencies. $\dot{g}$ and $\ddot{g}$ denote the first and the second derivatives of the dimensionless amplitude with respect the time variable, respectively.

According to the multiple scale method [36], the linear approximate solution of (12) is

$$g(\tau;\varepsilon) = g_0(T_0, T_1) + \varepsilon g_1(T_0, T_1) \tag{13}$$

where $T_0 = \tau$ and $T_1 = \varepsilon\tau$.

Substituting (13) into (12) and equating the coefficients of ε^0 and ε^1 on both sides, we obtain

$$\varepsilon^0: \quad \mathrm{D}_0^2 g_0 + g_0 = \eta_3(q_1 \cos\Omega_1 t + q_2 \cos\Omega_2 t) \tag{14}$$

$$\varepsilon^1: \quad \mathrm{D}_0^2 g_1 + g_1 = -2\mathrm{D}_0\mathrm{D}_1 g_0 - \tilde{\eta}_1 \mathrm{D}_0 g_0 - \tilde{\eta}_2 g_0^3 \tag{15}$$

where the partial differential operators are $\mathrm{D}_0 = \frac{\partial}{\partial T_0}$, $\mathrm{D}_1 = \frac{\partial}{\partial T_1}$ and $\mathrm{D}_0^2 = \frac{\partial^2}{\partial T_0^2}$, respectively.

The general solution of (14) can be written as

$$g_0 = A(T_1)\exp(\mathrm{i}T_0) + \Lambda_1 \exp(\mathrm{i}\Omega_1 T_0) + \Lambda_2 \exp(\mathrm{i}\Omega_2 T_0) + cc \tag{16}$$

where $A(T_1)$ is an undetermined function at this point. It will be determined by eliminating the secular terms from g_1. In (16), cc stands for the complex conjugate terms. Λ_n is denoted $\Lambda_n = \frac{\eta_3}{2} q_n (1 - \Omega_n^2)^{-1}$ and i is imaginary unit.

Substituting (16) into (15) gives

$$\begin{aligned}
&\mathrm{D}_0^2 g_1 + g_1 \\
&= -\big[\mathrm{i}(2A' + \tilde{\eta}_1 A) + 3\tilde{\eta}_2 A^2 \overline{A} + 6\tilde{\eta}_2 A \Lambda_1^2 \\
&\quad + 6\tilde{\eta}_2 A \Lambda_2^2\big]\exp(\mathrm{i}T_0) - \big[\mathrm{i}\Omega_1\tilde{\eta}_1 + 3\tilde{\eta}_2(2A\overline{A} \\
&\quad + \Lambda_1^2 + 2\Lambda_2^2)\big]\Lambda_1 \exp(\mathrm{i}\Omega_1 T_0) - \big[\mathrm{i}\Omega_2\tilde{\eta}_1 \\
&\quad + 3\tilde{\eta}_2(2A\overline{A} + 2\Lambda_1^2 + \Lambda_2^2)\big]\Lambda_2 \exp(\mathrm{i}\Omega_2 T_0) \\
&\quad - \tilde{\eta}_2 A^3 \exp(3\mathrm{i}T_0) - \tilde{\eta}_2 \Lambda_1^3 \exp(3\mathrm{i}\Omega_1 T_0) \\
&\quad - \tilde{\eta}_2 \Lambda_2^3 \exp(3\mathrm{i}\Omega_2 T_0) \\
&\quad - 3\tilde{\eta}_2 A^2 \Lambda_1 \exp\big[\mathrm{i}(2+\Omega_1)T_0\big] \\
&\quad - 3\tilde{\eta}_2 A^2 \Lambda_2 \exp\big[\mathrm{i}(2+\Omega_2)T_0\big] \\
&\quad - 3\tilde{\eta}_2 A^2 \Lambda_1 \exp\big[\mathrm{i}(2-\Omega_1)T_0\big] \\
&\quad - 3\tilde{\eta}_2 A^2 \Lambda_2 \exp\big[\mathrm{i}(2-\Omega_2)T_0\big] \\
&\quad - 3\tilde{\eta}_2 A \Lambda_1^2 \exp\big[\mathrm{i}(1+2\Omega_1)T_0\big] \\
&\quad - 3\tilde{\eta}_2 A \Lambda_2^2 \exp\big[\mathrm{i}(1+2\Omega_2)T_0\big] \\
&\quad - 3\tilde{\eta}_2 A \Lambda_1^2 \exp\big[\mathrm{i}(1-2\Omega_1)T_0\big] \\
&\quad - 3\tilde{\eta}_2 A \Lambda_2^2 \exp\big[\mathrm{i}(1-2\Omega_2)T_0\big] \\
&\quad - 6\tilde{\eta}_2 A \Lambda_1 \Lambda_2 \exp\big[\mathrm{i}(1+\Omega_1+\Omega_2)T_0\big] \\
&\quad - 6\tilde{\eta}_2 A \Lambda_1 \Lambda_2 \exp\big[\mathrm{i}(1-\Omega_1-\Omega_2)T_0\big] \\
&\quad - 6\tilde{\eta}_2 A \Lambda_1 \Lambda_2 \exp\big[\mathrm{i}(1-\Omega_1+\Omega_2)T_0\big] \\
&\quad - 6\tilde{\eta}_2 A \Lambda_1 \Lambda_2 \exp\big[\mathrm{i}(1+\Omega_1-\Omega_2)T_0\big] \\
&\quad - 3\tilde{\eta}_2 \Lambda_1^2 \Lambda_2 \exp\big[\mathrm{i}(2\Omega_1+\Omega_2)T_0\big] \\
&\quad - 3\tilde{\eta}_2 \Lambda_1^2 \Lambda_2 \exp\big[\mathrm{i}(2\Omega_1-\Omega_2)T_0\big] \\
&\quad - 3\tilde{\eta}_2 \Lambda_1 \Lambda_2^2 \exp\big[\mathrm{i}(\Omega_1+2\Omega_2)T_0\big] \\
&\quad - 3\tilde{\eta}_2 \Lambda_1 \Lambda_2^2 \exp\big[\mathrm{i}(2\Omega_2-\Omega_1)T_0\big] + cc
\end{aligned} \tag{17}$$

where an apostrophe indicates derivative of A with respect to τ.

We note that for the two-frequency excitation, where $\Omega_2 > \Omega_1$, the combination resonances can occur are $1 \approx \Omega_2 \pm 2\Omega_1$, $2\Omega_1 - \Omega_2$, $1 \approx 2\Omega_2 \pm \Omega_1$ and $1 \approx (\Omega_2 \pm \Omega_1)/2$.

In this paper, we consider the case in which $1 \approx (\Omega_2 + \Omega_1)/2$. We introduce a detuning parameter σ and let $1 = (\Omega_1 + \Omega_2)/2 - \varepsilon\sigma$. Then, according to (17), the secular terms will be eliminated if

$$\begin{aligned}
&\mathrm{i}(2A' + \tilde{\eta}_1 A) + 3\tilde{\eta}_2 A^2 \bar{A} + 6\tilde{\eta}_2 A \Lambda_1^2 + 6\tilde{\eta}_2 A \Lambda_2^2 \\
&\quad + 6\tilde{\eta}_2 \overline{A} \Lambda_1 \Lambda_2 \exp(\mathrm{i}2\sigma T_1) = 0
\end{aligned} \tag{18}$$

Letting $A = \frac{1}{2} a \exp(\mathrm{i}\theta)$ in (18), where a and θ are real, using the definition of Λ_n, and separating real and imaginary parts, we obtain

$$a' = -\frac{1}{2}\tilde{\eta}_1 a - \tilde{\eta}_2 \Gamma_2 a \sin\gamma \tag{19a}$$

$$a\gamma' = (2\sigma - 2\tilde{\eta}_2\Gamma_1)a - \frac{3}{4}\tilde{\eta}_2 a^3 - 2\tilde{\eta}_2 \Gamma_2 a \cos\gamma \tag{19b}$$

where

$$\Gamma_1 = \frac{3}{4}\eta_3^2\big[q_1^2\big(1-\Omega_1^2\big)^{-2} + q_2^2\big(1-\Omega_2^2\big)^{-2}\big]$$

$$\Gamma_2 = \frac{3}{4}\eta_3^2\big[q_1 q_2\big(1-\Omega_1^2\big)^{-1}\big(1-\Omega_2^2\big)^{-1}\big]$$

$$\gamma = 2\sigma T_1 - 2\theta$$

To find the bifurcation response equation, letting $a' = \gamma' = 0$ in (19) and then eliminating γ results in

the following algebraic equation:

$$a^4 + \zeta^2 + k_1 a^2 + k_2 = 0 \tag{20}$$

where

$$\zeta^2 = \left[\frac{8(\varepsilon\sigma - \eta_2\Gamma_1)}{3\eta_2}\right]^2$$
$$k_1 = -\frac{16(\varepsilon\sigma - \eta_2\Gamma_1)}{3\eta_2}$$
$$k_2 = \frac{16\eta_1^2}{9\eta_2^2} - \frac{64}{9}\Gamma_2^2$$

Taking the germ that $g_0(a,\zeta) = a^4 + \zeta^2$, where its codimension is 5, we have the universal unfolding [37, 38]

$$G(a,\zeta,\alpha_1,\alpha_2,\alpha_3,\alpha_4,\alpha_5) = a^4 + \zeta^2 + \alpha_1 a^2\zeta + \alpha_2 a\zeta + \alpha_3 a^2 + \alpha_4 a + \alpha_5 \tag{21}$$

where $\alpha_1, \alpha_2, \alpha_3, \alpha_4$, and α_5 are unfolding parameters.

It is very difficult to discuss the bifurcation behavior of (21) in full detail. Considering (20) and letting $\alpha_1 = \alpha_2 = \alpha_4 = 0, \alpha_3 = k_1, \alpha_5 = k_2$, we only analyze the engineering unfolding as follows:

$$G(a,\zeta,\alpha_3,\alpha_5) = a^4 + \zeta^2 + \alpha_3 a^2 + \alpha_5 \tag{22}$$

We know that transition set Σ of an universal unfolding $G : R \times R \times R^K \to R$ is formulated as follows (see p. 140 in Golubitsky and Schaeffer (1985)) [39]:

- Bifurcation point set

$$B = \{\alpha \in R^K : \text{there exists } (a,\zeta) \in R \times R \text{ such that } G = G_a = G_\zeta = 0 \text{ at } (a,\zeta,\alpha)\}$$

- Hysteresis set

$$H = \{\alpha \in R^K : \text{there exists } (a,\zeta) \in R \times R \text{ such that } G = G_a = G_{aa} = 0 \text{ at } (a,\zeta,\alpha)\}$$

- Double limit point set

$$D = \{\alpha \in R^K : \text{there exists } (a_1,a_2,\zeta) \in R \times R \times R, a_1 \neq a_2 \text{ such that } G = G_a = 0 \text{ at } (a_i,\zeta,\alpha), i = 1,2\}$$

- Transition set $\Sigma = B \cup H \cup D$

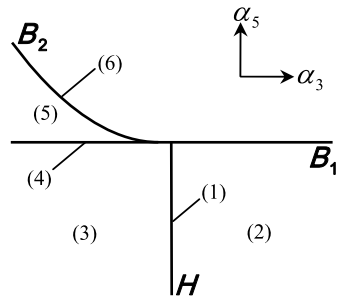

Fig. 2 The transition set in (α_3, α_5) plane

According to the singularity theory, the transition set of (22) is as follows:

(1) Bifurcation point set:

$$B_1 = \{\alpha_5 = 0\}$$
$$B_2 = \left\{\alpha_5 = \frac{1}{4}\alpha_3^2 \text{ and } \alpha_3 < 0\right\}$$

(2) Hysteresis set:

$$H = \{\alpha_3 = 0 \text{ and } \alpha_5 \leq 0\}$$

(3) Double limit point set:

$$D = \Phi \text{ (null set)}$$

From Fig. 2, we can see that the (α_3, α_5) parametric plane is divided by the transition set into four different regions. The six different topological structures of curves in different regions and in the transition set are shown in Fig. 3. According to the unfolding parameters, the bifurcation diagrams can be divided into two classes that are persistent and nonpersistent. Moreover, the bifurcation diagrams (2), (3), and (5) in Fig. 3 are persistent and the bifurcations are generic. It is indicated that the perturbed bifurcation diagrams in the universal unfolding (22) would remain unchanging if subjected to an additional small perturbation; the bifurcation diagrams (1), (4), and (6) in Fig. 3 are nonpersistent and the bifurcations are degenerate.

5 Numerical simulations of dynamic bifurcation

In the following investigation, the fourth-order Runge–Kutta algorithm is utilized to numerically analyze the periodic and chaotic motions of the FGM circular plate

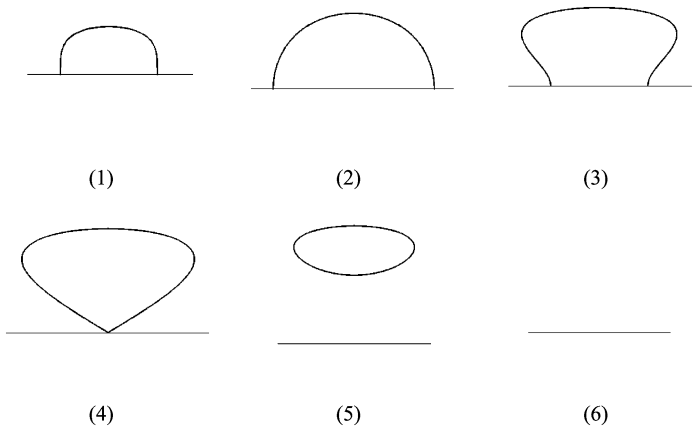

Fig. 3 The diagrams of static bifurcation

subjected to thermal and mechanical loads. The radius and thickness of the plate are $R = 0.3$ m and $h = 0.004$ m, respectively. The environmental temperature is $T_0 = 300$ K. The set of material mixture considered is zirconium oxide and titanium alloy, referred to as ZrO_2/Ti-6Al-4V. The upper surface of this FGM plate is metal-rich and the lower surface is ceramic-rich. The mass density and thermal conductivity are: $\rho_c = 3000$ kg/m^3, $\kappa_c = 1.80$ W/mK for ZrO_2; $\rho_m = 4429$ kg/m^3, $\kappa_m = 7.82$ W/mK for Ti-6Al-4V. Young's modulus and thermal expansion coefficients of these materials are assumed to be temperature-dependent and from the literature [40]. Poisson's ratio is assumed to be a constant for ZrO_2/Ti-6Al-4V $\mu = 0.3$ and the volume fraction index is $n = 200$. We consider the temperature over upper and lower surface is $\Delta T_m = 300$ K and $\Delta T_c = 370$ K, respectively. The first excitation frequency is $\Omega_1 = 0.4$ and the second load is $q_2 = 400$ N/m^2. The detuning parameter is assumed to be $\varepsilon\sigma = 0.01$. Changing the first load q_1, we obtain the dynamics of the FGM plate.

The global bifurcation diagram of the dynamical system is shown in Fig. 4. It denotes that the dimensionless vibration amplitude exists jump phenomenon with the change of the excitation q_1. In the case of $1 \approx (\Omega_2 + \Omega_1)/2$, it is obviously seen that the bifurcation with combination resonance is very complicated. The period response where period doubling occurs and chaotic response occur alternately. For clarity, we plot the enlarged bifurcation diagrams and corresponding them for the regions (1) and (2), as shown in Figs. 5 and 6, respectively. They indicate that the maximum Lyapunov exponent is $\lambda_{\max} < 0$ when the periodic motion occurs for the FGM plate and the maximum Lyapunov exponent is $\lambda_{\max} > 0$ when the chaos occurs for the FGM plate.

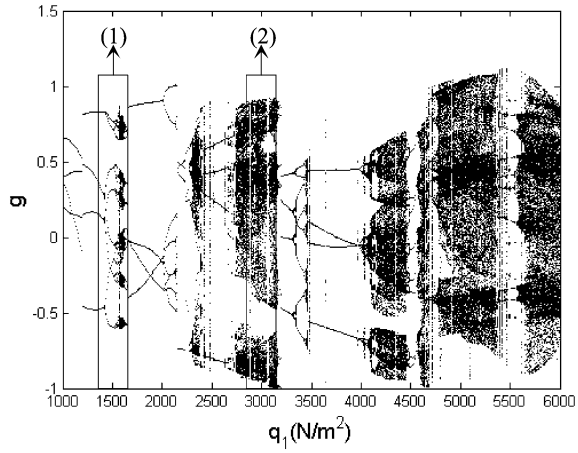

Fig. 4 The bifurcation for the load q_1

Here, considering the results of the figures (Figs. 5–6), we discuss the dynamical responses of the FGM plate with different excitation q_1 and obtain the phase portrait, Poincaré map, and Lyapunov exponent spectrum. Initially, the response of the system is given in Fig. 7 when the load is $q_1 = 1350$ N/m^2. Figure 7 (a) and (b), respectively, denote the phase portrait and Poincaré map. Figure 7(c) represents the Lyapunov exponents λ_1 and λ_2 evolving the dimensionless time τ. It can be shown that the Lyapunov exponent spectrum gradually became stabile and $\lambda_1 = \lambda_2 < 0$. Combining Fig. 7(b) with Fig. 7(c), we can know the phase portrait in Fig. 7(a) is period-4 attractor and the system exits period-4 motion. Increasing the excitation q_1, the pe-

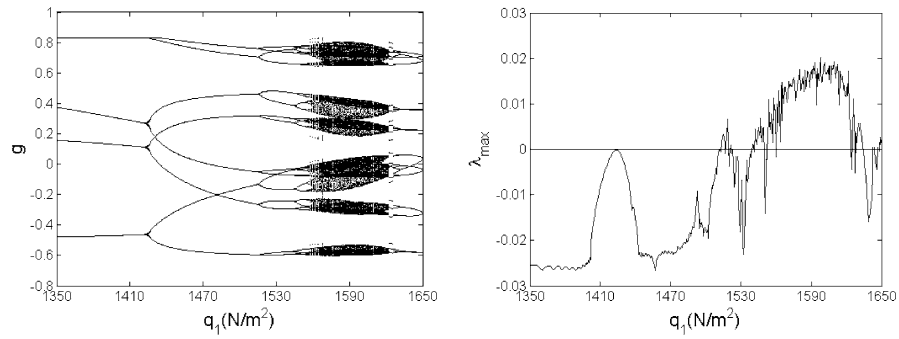

Fig. 5 The enlarged bifurcation diagram of region (1) and the corresponding maximum Lyapunov exponents

(a) Bifurcation diagram (b) Maximum Lyapunov exponents

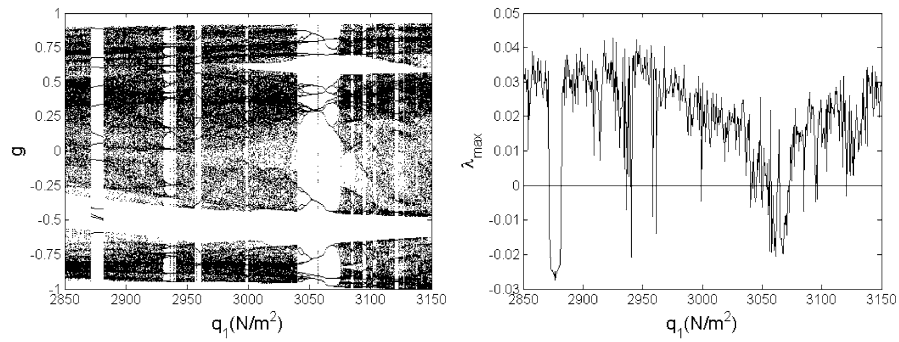

Fig. 6 The enlarged bifurcation diagram of region (2) and the corresponding maximum Lyapunov exponents

(a) Bifurcation diagram (b) Maximum Lyapunov exponents

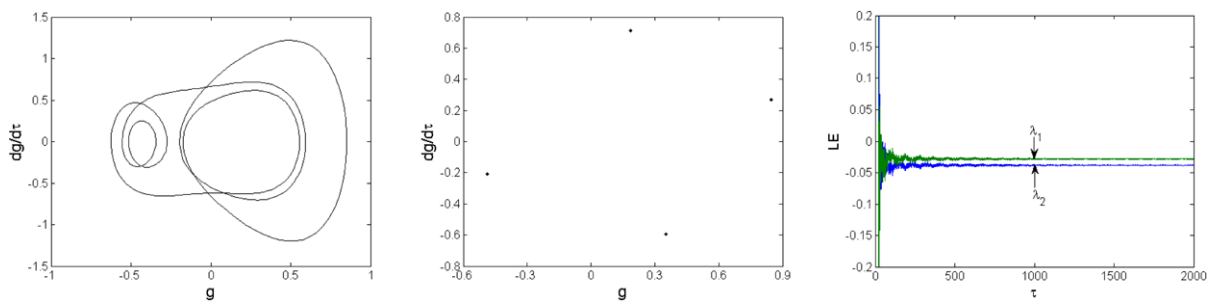

(a) The phase portrait (b) Poincaré map (c) Lyapunov exponent spectrum

Fig. 7 The period-4 motion of the system exists when $q_1 = 1350\ \mathrm{N/m^2}$

riod doubling bifurcation occurs near $q_1 = 1420\ \mathrm{N/m^2}$ and the motion becomes period-8 from period-4. For instance, the Poincaré map expresses eight points when $q_1 = 1470\ \mathrm{N/m^2}$ in Fig. 8. When the excitation is increased to $q_1 = 1520\ \mathrm{N/m^2}$, the period-16 motion can be found, as shown in Fig. 9. Continuously increasing the excitation to $q_1 = 1600\ \mathrm{N/m^2}$, Fig. 10 shows that the chaotic motions of the FGM plate occur and the stable Lyapunov exponent $\lambda_1 > 0$.

The results from the Fig. 4 show that when the forcing excitation q_1 is increasing, the system exists period doubling and chaotic motion. It can be seen clearly in Fig. 6. The figure illustrates that chaotic motions mostly occur in $[2850\ \mathrm{N/m^2}, 3150\ \mathrm{N/m^2}]$, however, many kinds of period doubling motion exist here. Figure 11 indicates that the period-12 motion of the FGM plate occur when the forcing excitation changes to $q_1 = 2875\ \mathrm{N/m^2}$. Figure 12 shows that the chaotic

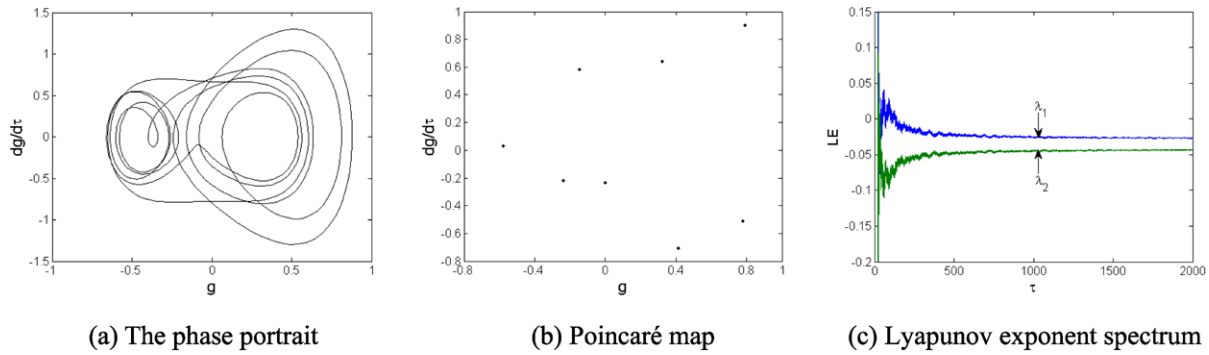

(a) The phase portrait (b) Poincaré map (c) Lyapunov exponent spectrum

Fig. 8 The period-8 motion of the system exists when $q_1 = 1470\ \mathrm{N/m^2}$

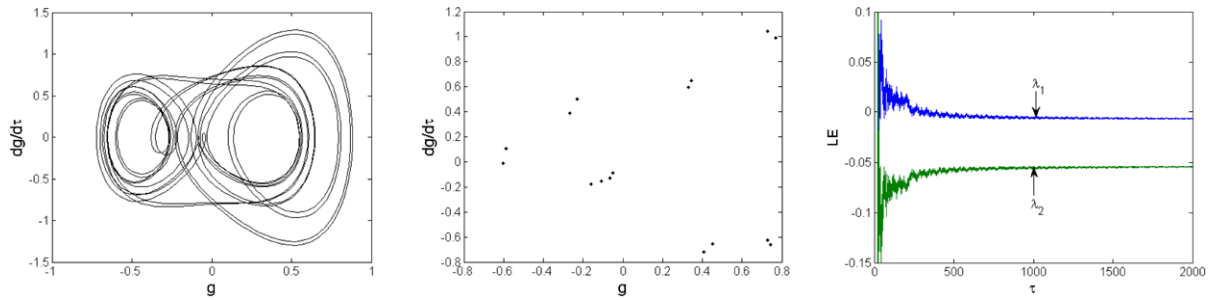

(a) The phase portrait (b) Poincaré map (c) Lyapunov exponent spectrum

Fig. 9 The period-16 motion of the system exists when $q_1 = 1520\ \mathrm{N/m^2}$

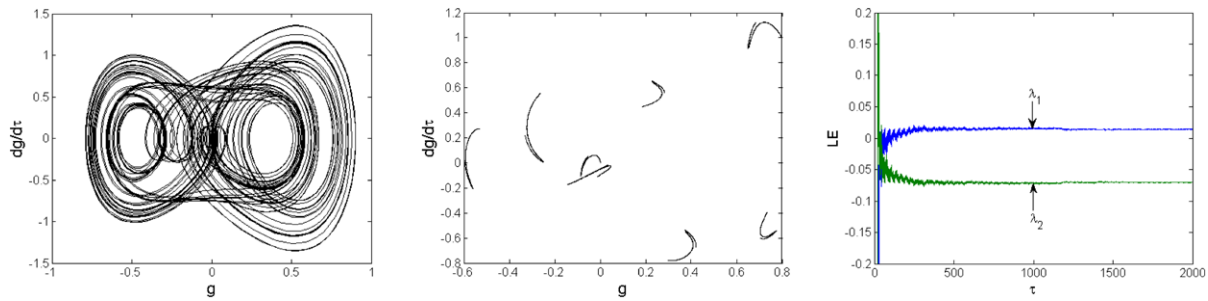

(a) The phase portrait (b) Poincaré map (c) Lyapunov exponent spectrum

Fig. 10 The chaotic motion of the system exists when $q_1 = 1600\ \mathrm{N/m^2}$

motion of the FGM plate again occurs when the forcing excitation changes to $q_1 = 2900\ \mathrm{N/m^2}$. It is found that a regular assemblage of black dots in Fig. 12(b) and the stable Lyapunov exponents $\lambda_1 > 0, \lambda_2 < 0$ in Fig. 12(c). When the excitation exceeds 4000 $\mathrm{N/m^2}$, the FGM plate mostly exists chaotic motions. For example, when the excitation is $q_1 = 5000\ \mathrm{N/m^2}$, the system occurs chaos, as shown in Fig. 13.

6 Conclusions

The bifurcation and chaotic dynamics of a circular FGM plate with combination resonance under two-term harmonic excitations are investigated. The nonlinear dynamic equations of FGM plate subjected to transverse harmonic excitation force and thermal load are derived using the principle of virtual work. The

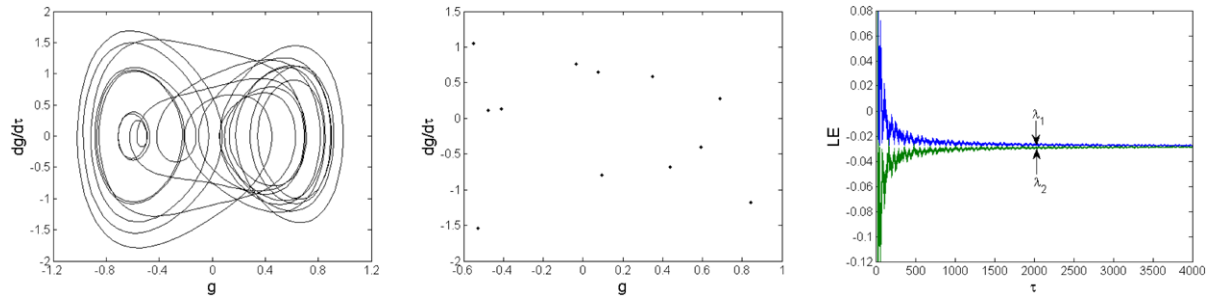

(a) The phase portrait (b) Poincaré map (c) Lyapunov exponent spectrum

Fig. 11 The period-12 motion of the system exists when $q_1 = 2875\ \mathrm{N/m^2}$

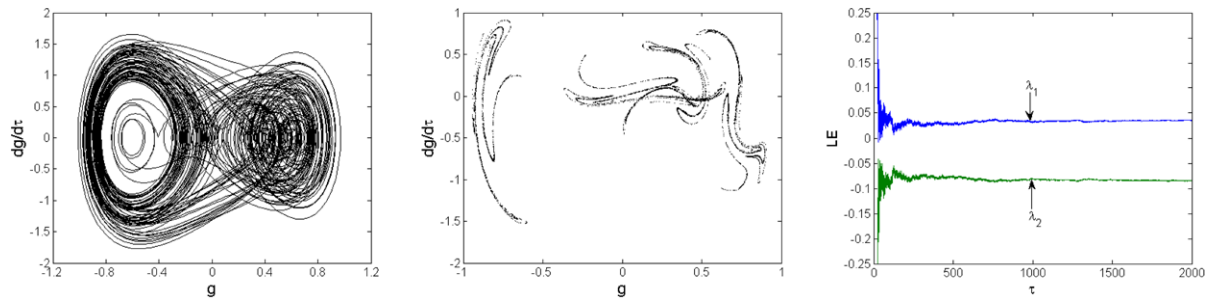

(a) The phase portrait (b) Poincaré map (c) Lyapunov exponent spectrum

Fig. 12 The chaotic motion of the system exists when $q_1 = 2900\ \mathrm{N/m^2}$

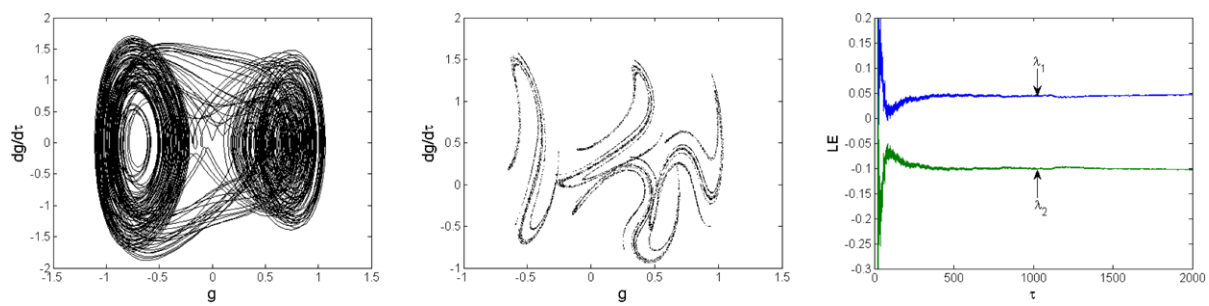

(a) The phase portrait (b) Poincaré map (c) Lyapunov exponent spectrum

Fig. 13 The chaotic motion of the system exists when $q_1 = 5000\ \mathrm{N/m^2}$

multiscale method is utilized to obtain the bifurcation equation. The universal unfolding problem of the bifurcation equation is studied using singularity theory. The bifurcation of the FGM plate is a high codimensional problem with codimension 5 and the singularity has complex bifurcation behaviors. Numerical simulation is carried out to investigate the dynamic bifurcation of the FGM plate and the influence of period doubling bifurcation with the change of an external excitation. The results obtained in this paper indicate that the FGM plate with combination resonance has complex dynamic behaviors and the period doubling response and chaotic response occurs alternately. The excitation can be considered to be a controlling force, which can control the responses of the circular FGM plate from the period-n motions to the chaotic motion.

Acknowledgements This work is supported by the Natural Science Foundation of the Hebei Province of China under Grant No. E2010001254.

References

1. Yamanouchi, M., Hirai, T., Shiota, I.: Overall view of the P/M fabrication of functionally gradient materials. In: Proceedings of the First International Symposium on Functionally Gradient Materials, Sendai, Japan, pp. 59–64 (1990)
2. Noda, N.: Thermal stresses in functionally graded materials. J. Therm. Stresses **22**, 477–512 (1999)
3. Reddy, J.N., Praveen, G.N.: Nonlinear transient thermo elastic analysis of functionally graded ceramic-metal plates. Int. J. Solids Struct. **35**, 4457–4476 (1998)
4. Liew, K.M., Yang, J., Kitipornchai, S.: Thermal post-buckling of laminated plates comprising FGM with temperature-dependent properties. J. Appl. Mech. **71**, 839–850 (2004)
5. Liew, K.M., Yang, J., Kitipornchai, S.: Postbuckling of piezoelectric FGM plates subject to thermo-electro-mechanical loading. Int. J. Solids Struct. **40**, 3869–3892 (2003)
6. Reddy, J.N.: Analysis of functionally graded plates. Int. J. Numer. Methods Eng. **47**, 663–684 (2000)
7. Liew, K.M., He, X.Q., Kitipornchai, S.: Finite element method for the feedback control of FGM shells in the frequency domain via piezoelectric sensors and actuators. Comput. Methods Appl. Mech. Eng. **193**, 257–273 (2004)
8. Hosseini Kordkheili, S.A., Naghdabadi, R.: Geometrically non-linear thermo-elastic analysis of functionally graded shells using finite element method. Int. J. Numer. Methods Eng. **72**(8), 964–986 (2007)
9. Zhao, X., Lee, Y.Y., Liew, K.M.: Mechanical and thermal buckling analysis of functionally graded plates. Compos. Struct. **90**, 161–171 (2009)
10. Reddy, J.N., Praveen, G.N.: Nonlinear transient thermoelastic analysis of functionally graded ceramic-metal plates. Int. J. Solids Struct. **35**(33), 4457–4476 (1998)
11. Ng, T.Y., Lam, K.Y., Liew, K.M.: Effect of FGM materials on the parametric resonance of plate structures. Comput. Methods Appl. Mech. Eng. **19**(8-10), 953–962 (2000)
12. Yang, J., Shen, H.S.: Free Vibration and parametric resonance of shear deformable functionally graded cylindrical panels. J. Sound Vib. **261**(5), 871–893 (2003)
13. Yang, J., Shen, H.S.: Dynamic response of initially stressed functionally graded rectangular thin plates. Compos. Struct. **54**(4), 497–508 (2001)
14. Vel, S.S., Batra, R.C.: Three-dimensional exact solutions for the vibration of functionally graded rectangular plate. J. Sound Vib. **272**, 703–730 (2004)
15. Liew, K.M., He, X.Q., Ng, T.Y., Kitipornchai, S.: Finite element piezothermoelasticity analysis and the active control of FGM plates with integrated piezoelectric sensors and actuators. Comput. Mech. **31**, 350–358 (2003)
16. Allahverdizadeh, A., Naei, M.H., Bahrami, M.N.: Nonlinear free and forced vibration analysis of thin circular functionally graded plates. J. Sound Vib. **310**(4–5), 966–984 (2008)
17. Zhao, X., Liew, K.M.: Geometrically nonlinear analysis of functionally graded plates using the element-free kp-Ritz method. Comput. Methods Appl. Mech. Eng. **198**, 2796–2811 (2009)
18. Zhao, X., Lee, Y.Y., Liew, K.M.: Thermoelastic and vibration analysis of functionally graded cylindrical shells. Int. J. Mech. Sci. **51**, 694–707 (2009)
19. Hao, Y.X., Chen, L.H., Zhang, W.: Nonlinear oscillations, bifurcations and chaos of functionally graded materials plate. J. Sound Vib. **312**(4–5), 862–892 (2008)
20. Yang, J., Hao, Y.X., Zhang, W., Kitipornchai, S.: Nonlinear dynamic response of a functionally graded plate with a through-width surface crack. Nonlinear Dyn. **59**, 207–219 (2010)
21. Sridhar, S., Mook, D.T., Nayfeh, A.H.: Non-linear resonances in the forced responses of plates, part I: symmetric responses of circular plates. J. Sound Vib. **41**, 359–373 (1975)
22. Hadian, J., Nayfeh, A.H.: Modal interaction in circular plates. J. Sound Vib. **142**, 279–292 (1990)
23. Feng, Z.C., Sethna, P.R.: Global bifurcations in the motion of parametrically excited thin plate. Nonlinear Dyn. **4**, 389–408 (1993)
24. Chang, S.I., Bajaj, A.K., Krousgrill, C.M.: Non-linear vibrations and chaos in harmonically excited rectangular plates with one-to-one internal resonance. Nonlinear Dyn. **4**, 433–60 (1993)
25. Liu, C.F., Chen, G.T.: Geometrically nonlinear axisymmetric vibrations of polar orthotropic circular plates. Int. J. Mech. Sci. **3**, 325–333 (1996)
26. Zhang, W., Liu, Z.M., Yu, P.: Global dynamics of a parametrically and externally excited thin plate. Nonlinear Dyn. **24**(3), 245–268 (2001)
27. Haterbouch, M., Benamar, R.: The effects of large vibration amplitudes on the axisymmetric mode shapes and natural frequencies of clamped thin isotropic circular plates. Part I: Iterative and explicit analytical solution for nonlinear transverse vibrations. J. Sound Vib. **265**, 123–154 (2003)
28. Haterbouch, M., Benamar, R.: The effects of large vibration amplitudes on the axisymmetric mode shapes and natural frequencies of clamped thin isotropic circular plates. Part II: Iterative and explicit analytical solution for nonlinear coupled transverse and in-plane vibrations. J. Sound Vib. **277**, 1–30 (2004)
29. Haterbouch, M., Benamar, R.: Geometrically nonlinear free vibrations of simply supported isotropic thin circular plates. J. Sound Vib. **280**, 903–924 (2005)
30. Akour, S.N., Nayfeh, J.F.: Nonlinear dynamics of polar-orthotropic circular plates. Int. J. Struct. Stab. Dyn. **6**, 253–268 (2006)
31. Zhang, W., Zhang, J.H., Yao, M.H.: The extended Melinkov method for non-autonomous nonlinear dynamical systems and application to multi-pulse chaotic dynamics of a buckled thin plate. Nonlinear Anal., Real World Appl. **11**, 1442–1457 (2010)
32. Touzé, C., Thomas, O., Amabili, M.: Transition to chaotic vibrations for harmonically forced perfect and imperfect circular plates. Int. J. Non-Linear Mech. **46**, 234–246 (2011)
33. Parker, T.S., Chua, L.O.: Practical Numerical Algorithms for Chaotic Systems. Springer, New York (1989)

34. Touloukian, Y.S.: Thermophysical Properties of High Temperature Solid Materials. McMillan, New York (1967)
35. Shen, H.S.: Thermal postbulking behavior of shear deformable FGM plates with temperature-dependent properties. Int. J. Mech. Sci. **49**(4), 466–47 (2007)
36. Nayfeh, A.H., Mook, D.T.: Nonlinear Oscillations. Wiley-Interscience, New York (1979)
37. Xu, K.Y., Cheng, C.J.: The Subharmonic bifurcation of a viscoelastic circular cylindrical shell. Nonlinear Dyn. **17**, 159–171 (1998)
38. Chen, F.Q., Liang, J.S., Chen, Y.S., et al.: Bifurcation analysis of an arch structure with parametric and forced excitation. Mech. Res. Commun. **34**, 213–221 (2007)
39. Golubitsky, M., Schaeffer, D.G.: Singularities and Groups in Bifurcation Theory, vol. I. Springer, New York (1985)
40. Reddy, J.N., Chin, C.D.: Thermomechanical analysis of functionally graded cylinders and plates. J. Therm. Stresses **21**(6), 593–629 (1998)